ZC3H11A mutations cause high myopia by triggering PI3K-AKT and NF-κB mediated signaling pathway in humans and mice

Chong Chen[1,2,3#], Qian Liu[1,2,3#], Cheng Tang[1,2,3#], Yu Rong[1,2,3], Xinyi Zhao[1,2,3], Dandan Li[1,2,3], Fan Lu[1,2,3]*, Jia Qu[1,2,3*], Xinting Liu[1,2,3]*

[1]National Engineering Research Center of Ophthalmology and Optometry, Eye Hospital, Wenzhou Medical University, Wenzhou, 325027, China;

[2]National Clinical Research Center for Ocular Diseases, Eye Hospital, Wenzhou Medical University, Wenzhou, 325027, China;

[3]State Key Laboratory of Ophthalmology, Optometry and Visual Science, Eye Hospital, Wenzhou Medical University, Wenzhou, 325027, China.

*For correspondence: liuxt@eye.ac.cn; qujia@eye.ac.cn; lufan62@eye.ac.cn

[#] These authors contributed equally to this work.

Abstract

High myopia (HM) is a severe form of refractive error that results in irreversible visual impairment and even blindness. However, the genetic and pathological mechanisms underlying this condition are not yet fully understood. From a cohort of 1015 patients with high myopia in adolescents, likely pathogenic missense mutations were identified in the *ZC3H11A* gene in four patients by whole exome sequencing. This gene is a zinc finger and stress-induced protein that plays a significant role in regulating nuclear mRNA export. To better understand the function and molecular pathogenesis of myopia in relation to gene mutations, a *Zc3h11a* knock-out (KO) mouse model was created. The heterozygous KO (Het-KO) mice exhibited significant shifts in refraction towards myopia. Myopia-related factors, including TGF-β1, MMP-2 and IL-6 were found to be upregulated in the retina or sclera, and electroretinography and immunofluorescence staining results showed dysfunction and reduced number of bipolar cells in the retina. Transmission electron microscopy findings suggesting ultrastructural abnormalities of the retina and sclera. Retinal transcriptome sequencing showed that 769 genes were differentially expressed, and *Zc3h11a* was found to have a negative impact on the PI3K-AKT and NF-κB signaling pathways by quantitative PCR and western blotting. In summary, this study characterized a new candidate pathogenic gene associated with

high myopia, and indicated that the ZC3H11A protein may serve as a stress-induced nuclear response trigger, and its abnormality causes disturbances in a series of inflammatory and myopic factors. These findings offer potential therapeutic intervention targets for controlling the development of HM.

Introduction

Myopia is a highly prevalent eye affliction that commonly develops during childhood and early adolescence. The prevalence of myopia among the adult population ranges from 10-30%, while parts of East and Southeast Asia have reported rates as high as 80-90% among young people (Baird et al., 2020; Holden et al., 2016). HM is a severe refractive error characterised by a diopter ≤ -6.00 D or an axial length greater than 26 mm. It is estimated that by 2050, the number of people with HM worldwide will reach 938 million, accounting for 9.8% of the total population. HM can trigger a range of adverse ocular changes, such as cataracts, glaucoma, retinal detachment, macular degeneration and possibly total blindness (Koga et al., 2014; Saw et al., 2005). While conventional methods for the prevention and control of myopia can provide some correction, they are not entirely effective in managing its progression, particularly during childhood and adolescence.

With the development of next-generation sequencing, whole exome sequencing (WES) and whole genome sequencing (WGS) have extended the findings of linkage studies to identify potential causes of syndromic HM (sHM) and non-syndromic HM (nsHM). To date, approximately 20 genes with causal associations have been identified in sHM, including *ZNF644, SCO2, CCDC111, LRPAP1, SLC39A5, LEPREL1, P4HA2, OPN1LW, ARR3, BSG, NDUFAF7, CPSF1, TNFRSF21, DZIP1, XYLT1, CTSH, GRM6, LOXL3* and *GLRA2* (Haarman et al., 2022; Tian et al., 2023; Yang et al., 2023; Ye et al., 2023). These discoveries have provided insight into the molecular mechanisms underlying HM. However, known candidate genes can only explain about 20% of the causes of this disease (Cai et al., 2019; Tedja et al., 2019). At the same time, the neuromodulators and signal molecules of HM are extremely complex, including sclera extracellular matrix (ECM) remodelling and endoplasmic reticulum (ER) stress (Ikeda

et al., 2022), inflammatory responses, the release of dopamine and gamma-aminobutyric acid (GABA), or abnormalities in myopia-related signaling pathways, such as retinoic acid signaling, TGF-β signaling and HIF-1α signaling.

Screening mutations from an in-house adolescents high myopia survey cohort by WES, we identified zinc finger CCCH domain-containing protein 11A (*ZC3H11A*) as a HM candidate gene. This particular gene is a member of the zinc finger protein gene family. Multiple zinc finger protein genes (e.g., *ZNF644, ZC3H11B, ZFP161, ZENK*) are associated with myopia or HM. Of these, *ZC3H11B* (a human homolog of *ZC3H11A*) and five GWAS loci (Schippert et al., 2007; Shi et al., 2011; Szczerkowska et al., 2019; Tang et al., 2020; Wang et al., 2004) correlate with AL elongation or HM severity. Proteomic studies further suggest ZC3H11A involvement in the TREX complex, implicating RNA export mechanisms in myopia pathogenesis. Additionally, it has been suggested that this protein is involved in stress-induced responses (Younis et al., 2018). Dysfunction of *ZC3H11A* results in enhanced NF-κB signaling through defective IκBα protein expression, which is accompanied by upregulation of numerous innate immune- and inflammation-related mRNAs, including *IL-8, IL-6* and *TNF* in vitro (Jimi et al., 2019). Moreover, patients with myopia have a higher proportion of inflammation-associated cells, including neutrophils, while those with moderate myopia show strained immune system function (Lin et al., 2016; Qi et al., 2022). Conversely, some traditional Chinese medicines can control myopia progression by suppressing AKT and NF-κB mediated inflammatory reactions (Chen et al., 2022). However, the precise pathological mechanism of *ZC3H11A* in myopia development remains unclear, necessitating further research.

The current study identified four variants in the *ZC3H11A* gene among a high myopia adolescent cohort of 1015 adolescents. Additionally, heterozygous knockout（Het-KO）mice were constructed using the CRISPR/Cas9 system and their myopic phenotypes, visual function, bipolar cell apoptosis, and retinal and scleral microstructure were assessed. Moreover, RNA sequencing and expression experiment was performed to identify perturbed molecules and pathways and to examine the interactions between

these factors in relation to HM. The above results will provide new ideas for the prevention and control of high myopia, especially early-onset, uncorrectable and familial myopia.

Results

ZC3H11A mutations are associated with HM in a Chinese cohort

The genomic data is sourced from an independently established genetic cohort of high myopia patients. Four missense mutations in the *ZC3H11A* gene (c.412G>A, p.V138I; c.128G>A, p.G43E; c.461C>T, p.P154L; and c.2239T>A, p.S747T) were identified in the 1015 HM patients aged from 15 to 18 years. The uncorrected visual acuity (UCVA) and axial length of these patients are presented in Table 1. All of the identified mutations exhibited very low frequencies in the Genome Aggregation Database (gnomAD) and Clinvar, and using pathogenicity prediction software SIFT, PolyPhen2, and CADD, most of them display high pathogenicity levels. Among them, c.412G>A, c.128G>A and c.461C>T were located in or around a domain named zf-CCCH_3 (Figure 1A and B). Furthermore, all of the mutation sites were located in highly conserved amino acids across different species (Figure 1C). Four mutations resulted in a higher degree of conformational flexibility and altered the negative charge at the corresponding sites (Figure 1D and E).

Zc3h11a Het-KO mice exhibited myopic phenotypes

Het-KO mice were constructed at four weeks of age against a C57BL/6J background using CRISPR/Cas9 technology (Supplement Figure 1). Retinal fundus images and ocular histomorphology of *Zc3h11a* Het-KO mice at eight weeks postnatal were assessed against those of their wild-type (WT) counterparts. No significant structural differences were observed (Supplement Figure 2). These findings suggest that the deletion of *Zc3h11a* does not alter the retinal structure or ocular histomorphology. Therefore, *Zc3h11a* Het-KO mice are a relevant model for the investigation of the role of *Zc3h11a* in refractive development.

Refraction and axial length in *Zc3h11a* Het-KO mice were found to be significantly

121 greater than in WT littermates (independent samples t-test, $p<0.05$; Figure 2A and B).
122 The difference between the two genotypes was statistically significant at weeks 4 and
123 6. Correspondingly, the vitreous chamber depth of *Zc3h11a* Het-KO mice was deeper
124 than that of WT littermates (independent samples t-test, $p<0.05$; Figure 2C). There were
125 no significant differences in the anterior chamber depth, lens diameter and body weight
126 between the two groups (Figure 2D-F). These results suggest that the Het-KO of the
127 *Zc3h11a* gene can lead to an increase in myopia in mice.
128

129 **Reduced b-wave amplitude and bipolar cell-labelled protein abundance in**
130 ***Zc3h11a* Het-KO mice**

131 To confirm if *Zc3h11a* is responsible for refractive development regulation, visual
132 function was assessed by electroretinography (ERG). Upon dark adaptation, b-wave
133 amplitudes in seven-week-old Het-KO mice were significantly lower at dark 3.0 (0.48
134 log cd·s/m²) and dark 10.0 (0.98 log cd·s/m²) compared to WT mice (Figure 3A and C).
135 On the contrary, there were no differences in a-wave amplitudes between the Het-KO
136 and WT groups (Figure 3B). Based on the ERG results, variations between Het-KO and
137 WT littermates can be observed. Under the dark adaptation conditions of 3.0 and 10.0,
138 there was a significant change in the amplitude of ERG b-waves, indicating impaired
139 bipolar cell function. Immunofluorescence analyses were performed on frozen retinal
140 sections to investigate this phenomenon further. Specifically, Zc3h11a, PKCα, Opsin-1
141 and Rhodopsin markers were utilised to detect the Zc3h11a protein, rod-bipolar cells,
142 cone cells and rod cells, respectively (Figure 3D-F). Quantitative analysis of
143 immunofluorescence staining results revealed that the protein abundance of Zc3h11a
144 and PKCα was significantly reduced in the Het-KO group (Figure 3G, H). Western blot
145 analysis further showed that the expression level of PKC-α protein in the retina of Het-
146 KO mice was significantly reduced, indicating a decrease in the number of bipolar cells
147 (Figure 3I, J). However, there were no significant differences in the protein abundance
148 of Opsin-1 and Rhodopsin between the two groups (Supplement Figure 3). Thus, both
149 the function and number of retinal bipolar cells were decreased in *Zc3h11a* Het-KO
150 mice.

151 **Retinal ultrastructure alterations in *Zc3h11a* Het-KO mice model**

152 Transmission electron microscopy (TEM) was used to analyse retinal ultrastructure of
153 in 10-week-old mice. In the inner nuclear layer (INL) of the retina, in contrast to WT
154 mice, Het-KO mouse cells had enlarged perinuclear gaps (black arrow), perinuclear
155 cytoplasmic oedema (blue arrow), and thinned and lightened cytoplasm (Figure 4A and
156 B). However, in the outer nuclear layer (ONL), no significant difference in cell
157 morphology was observed between the two groups of mice (Figure 4C and D). These
158 findings indicate structural damage to bipolar cells in Het-KO mice. Furthermore, when
159 compared to the WT group, the Het-KO mice exhibited relatively damaged
160 photoreceptor cell membrane discs (MB), in which the outer layer was detached and
161 sparsely distributed locally (Figure 4E and F). There were also a small number of
162 broken membrane discs, as well as some disorganized and loosely arranged ones (red
163 arrow), with a slight increase in size (Figure 4G and H). This suggests impaired light
164 signal capture, transduction, and compromised visual function in Het-KO mice.

165

166 **RNA-Seq analysis of molecular and pathways changes in *Zc3h11a* Het-KO mice**
167 **retinas**

168 In the retina transcriptome analysis, 769 genes were differentially expressed (Fold
169 change (FC) of at least two and a P value < 0.05) in the *Zc3h11a* Het-KO group, of
170 which, 303 were upregulated and 466 were downregulated (Figure 5A). GO enrichment
171 analysis revealed significant enrichment of differentially expressed genes in the
172 following functions: Zinc ion transmembrane transport (GO:0071577) within metal ion
173 homeostasis, associated with retinal photoreceptor maintenance (Ugarte and Osborne,
174 2001), RNA biosynthesis and metabolism (GO:0006366) in transcriptional regulation,
175 potentially influencing ocular development, negative regulation of NF-κB signaling
176 (GO:0043124) in inflammatory modulation, a pathway involved in scleral remodelling
177 (Xiao et al., 2025), calcium ion binding (GO:0005509), critical for phototransduction
178 (Krizaj and Copenhagen, 2002), zinc ion transmembrane transporter activity
179 (GO:0005385), participating in retinal zinc homeostasis (Figure 5B and C). KEGG
180 pathway enrichment analysis indicated that the differentially expression genes (DEGs)

in the *Zc3h11a* Het-KO group were primarily involved in the PI3K-AKT signaling pathway, MAPK signaling pathway, and neuropsychiatric disease (Figure 5D). These findings preliminarily suggest dysregulated NF-κB and PI3K-AKT signaling pathways in the retinas of *Zc3h11a* Het-KO mice.

_Zc3h11a_ negatively regulates the PI3K-AKT and NF-κB pathways

PI3K-AKT is one of the most important pathways for cell survival, division, autophagy and differentiation (Alzahrani, 2019). Meanwhile, it has been found that *ZC3H11A* can regulate the NF-κB pathway at the level of *IκBα* mRNA export in ZC3-KO cells (Darweesh et al., 2022). IκBα is a critical protein that governs NF-κB function predominantly within the cytoplasmic compartment. It plays a pivotal role in inhibiting the activation of NF-κB (Dyson and Komives, 2012; Manavalan et al., 2010). In addition, AKT promotes IκBα phosphorylation to undergo degradation, which enhances the nuclear translocation of NF-kB (Alzahrani, 2019; Torrealba et al., 2020). Based on RNA sequencing and the aforementioned literature evidence, this study investigated the regulatory role of *Zc3h11a* in the PI3K-AKT and NF-κB pathways within the mouse retina. To this end, we evaluated the mRNA and protein expression levels of Zc3h11a, PI3K, AKT, p-AKT, IκBα and NF-κB in the retina. The expression levels ofPI3K, AKT, p-AKT and NF-κB were significantly upregulated, while Zc3h11a and IκBα was downregulated in Het-KO mice (Figure 6A-L). Meanwhile, through transfection of overexpression mutant plasmids, it was found that compared to the wild-type, the mRNA expression levels of *IκBα* in the nucleus of all four mutant types ($ZC3H11A^{V138I}$, $ZC3H11A^{G43E}$, $ZC3H11A^{P154L}$ and $ZC3H11A^{S747T}$) were significantly reduced (Supplement Figure 4). These results strongly suggest that *ZC3H11A* likely contributes to myopia pathogenesis by inhibiting both PI3K-AKT and NF-κB signaling pathways.

TGF-β1, MMP-2 and IL-6 were increased in _Zc3h11a_ Het-KO mice

In animal models of myopia, it has been established that intraocular concentrations of TGF-β1 are elevated (Chen et al., 2013; Liu et al., 2022), especially in the retina and sclera. The abnormal expression of matrix metalloproteinase-2 (MMP-2) and

interleukin-6 (IL-6) can induce myopia, and these are regulated by NF-κB (Libermann and Baltimore, 1990; Wu and Schmid-Schönbein, 2011). qPCR analysis showed increased expression of *TGF-β1*, *MMP-2*, and *IL-6* in the sclera and retina of Het-KO mice compared with WT mice (Figure 7A and B). The western blot results showed increased expression levels of TGF-β1 and MMP-2 in the retinas of *Zc3h11a* Het-KO mice (Figure 7D).Scleral TEM results suggested that scleral collagen fibres in Het-KO mice were disorganized over a large area with irregular transverse and longitudinal arrangement (Figure 7C). These results further corroborate that Zc3h11a Het-KO mice exhibit a myopic phenotype, and that Zc3h11a mutation may participate in the development of myopia by inhibiting the NF-κB signaling pathway, thereby upregulating the expression of myopia-related factors such as MMP-2, and IL-6.

Discussion

This study identified and validated a new candidate gene in a large high myopia cohort, *ZC3H11A*. Moreover, the study provided evidence of the presence of moderate or HM phenotypes and damaged bipolar cells *in vivo* by constructing Het-KO mice for the first time. TEM analysis showed ultrastructural changes in parts of both the retina and sclera of Het-KO mice. To understand how *ZC3H11A* regulates the development of HM, retinal transcriptome sequencing was performed. The results revealed that *Zc3h11a* mutation upregulates the PI3K-AKT and NF-κB signaling pathways. In addition, the expression levels of myopia-related factors, such as TGF-β1, MMP-2 and IL-6, were upregulated in the retina and sclera of the Het-KO mice. Therefore, it can be speculated that the ZC3H11A protein may act as a stress-induced nuclear response trigger, its abnormal expression contributing to the early onset of HM.

ZC3H11A is involved in the export and post-transcriptional regulation of selected mRNA transcripts required to maintain metabolic processes in embryonic cells, these are essential for the viability of early mouse embryos (Younis et al., 2023). In studies of chickens, mice and humans, the zinc finger protein *ZENK* was found to play a role in the development of refractive myopic excursion and lengthening of the ocular axis. Moreover, early growth response gene type 1 Egr-1 (the human homolog of *ZENK*)

activates the TGF-β1 gene by binding to its promoter, which is thought to be associated with myopia (Baron et al., 2006; Xiao et al., 2022). Another zinc protein finger protein 644 isoform, *ZNF644*, has recently been identified by WES as causing HM in Han Chinese families (Shi et al., 2011). *ZC3H11A* is also a zinc finger protein, and the findings of the current study revealed that *Zc3h11a* Het-KO mice showed a myopic shift, which is consistent with previous studies reporting reduced protein expression of *Zc3h11a* in an unilateral induced myopic mouse model (Fan et al., 2012).

In vertebrate models, refractive development and ocular axial growth are visually controlled (Wallman and Winawer, 2004). The regulation of axial length or refractive error occurs through complex light-dependent retina-to-sclera signaling (Tkatchenko and Tkatchenko, 2019). Optical scatter information is processed by the retina and then converted into molecular signals that regulate peripheral retinal growth and scleral connective tissue renewal, ultimately affecting the growth rate of the posterior segment of the eye (Harper and Summers, 2015; Tkatchenko et al., 2006; Tkatchenko et al., 2018). All cell types of the retina contain myopia-related genes and retinal circuitry driving refractive error. In this study, Het-KO mice were found to have reduced b-wave amplitudes, diminished the abundance of PKCα and ultrastructural changes in inner nuclear layer (INL) of the retina. Thus, damage to retinal bipolar cells may impair visual signal processing and transduction through neural circuit alterations, thereby contributing to the pathogenesis of HM.

Transcriptome sequencing and quantitative analyses collectively demonstrated downregulated PI3K-AKT and NF-κB signaling pathways in the retinas of Het-KO mice. Given the well-established dysregulation of these pathways in high myopia (Lin et al., 2016), we aimed to investigate how *Zc3h11a* mediates alterations in these pathways and their potential regulatory cross-talk in the mouse retina. Previous research revealed that a decrease in *Zc3h11a* inhibited the translocation of *IκBα* from the nucleus to the cytoplasm (Darweesh et al., 2022). *IκBα* is a downstream factor of PI3K-AKT and binds to NF-κB (p65) in the cytoplasm, inhibiting its nuclear translocation. The qPCR and western Blot results verified that *Zc3h11a* mutation negatively regulates both the PI3K-AKT and NF-κB signaling pathways. Thus, *Zc3h11a* may exert an influence

on PI3K-AKT and NF-κB signaling pathways by modulating the cytoplasmic levels of IκBα, contributing to the development of myopia.

NF-κB was first discovered 25 years ago and described as a key regulator of induced gene expression in the immune system, playing a central role in the coordinated control of intrinsic immune and inflammatory responses (Hayden and Ghosh, 2011; Morgan and Liu, 2011). The downstream factors of this pathway include IL-6, IL-8, TNF-α, MMP-2, TGF-β1, etc (Jimi et al., 2019; Yoshida and Whitsett, 2006). Studies have demonstrated that the MMP-2 and IL-6 expression levels are increased in myopic eyes and that inhibiting MMP-2 or IL-6 expression will provide some degree of control over myopia progression (Lin et al., 2016; Zhao et al., 2018). Identification of the PI3K-AKT-NF-κB signaling pathway and downstream myopia effect in our study may open up new opportunities for the prevention and treatment of HM and fundus lesions in the future.

There are a number of limitations of this study that should be acknowledged. First, the patient's ophthalmic examination was not comprehensive enough, and genetic analysis such as segregation analysis was not performed. Second, Zc3h11a homozygous KO (Homo-KO) mice were not obtained in our study because homozygous deletion of exons confer embryonic lethality (Younis et al., 2023). Third, the axial length of Zc3h11a Het-KO mice was longer only at 4 and 6 weeks of age. This may be due to the small size of mouse eyes (1D refractive change corresponds to only 5-6μm axial length change) (Schaeffel., 2004) and the theoretical resolution limit of 6μm of the SD-OCT equipment used in this study (Zhou., 2008b). Fourth, while the current study observed damage to bipolar cells in Het-KO mice, an in-depth exploration of the underlying mechanism was beyond the scope of the research. Finally, there was a limited observation time in this study and the effect of *ZC3H11A* on the late refractive system was not assessed.

Overall, this study has provided four key findings. First, it was confirmed that the *ZC3H11A* is a new candidate gene associated with HM in a cohort of Chinese Han individuals. Secondly, changes in *Zc3h11a* expression were found to affect retinal function, particularly in bipolar cells. Third, changes in *Zc3h11a* expression were found

to cause alterations in numerous signaling pathways, the most notable being the PI3K-AKT and NF-κB pathways. Fourth, changes in *Zc3h11a* expression were found to cause changes in the myopia-related genes TGF-β1, MMP-2 and IL-6. The above results suggest that abnormal expression of *Zc3h11a* triggers nuclear translocation defects of *IκBα*, thereby exerting negative feedback regulation of the PI3K-AKT signaling pathway and inhibiting the NF-κB signaling pathway. At the same time, the increase in TGF-β1 in myopic eyes stimulates the PI3K-AKT signaling pathway, which leads to activation of the PI3K-AKT signaling pathway, resulting in downstream degradation of IκBα after phosphorylation. This, in turn, increases the nuclear translocation of NF-κB. To sum up, *Zc3h11a* promotes the myopia-associated factor TGF-β1 by acting directly or indirectly on both the PI3K-AKT and NF-κB signaling pathway-mediated stress reactions and the expression of MMP-2 and IL-6, which together, caused the development of early high myopia (Figure 8). Therefore, this model can be used as one of the new strategies for intervention and treatment of high myopia. However, because the causes of myopia or HM are complex and involve different tissues and molecular pathways in the eye, it is likely that future research will identify more genes and molecular mechanisms that could provide guidance for clinical intervention and treatment.

Materials and methods

Ethics approval and consent to participate

The studies that involved human participants were approved by the Eye Hospital, Wenzhou Medical University (Wenzhou, China), and were carried out in strict adherence to the guidelines of the Helsinki Declaration. All participants provided informed consent. Furthermore, all animal experiments were approved by the Animal Care and Ethics Committee at Wenzhou Medical University and were performed according to the guidelines set forth in the Association for Research in Vision and Ophthalmology Statement for the Use of Animals in Ophthalmic and Visual Research. (https://www.arvo.org/About/policies/statement-for-the-use-of-animals-in-ophthalmic-and-vision-research/).

Recruitment of subjects

Four sporadic HM patients (aged from 15-18) were recruited from the Eye Hospital of Wenzhou Medical University, three of them come from the Myopia Associated Genetics and Intervention Consortium (MAGIC) project. HM was defined as SE ≤ -6.00 D in either eye (Flitcroft et al., 2019). Partial patients underwent certain ophthalmic examinations, including visual acuity (at least three measurements under non-cycloplegia), axial length and fundus photography were performed.

WES and the detection of variants

DNA was extracted from all probands using a FlexiGene DNA Kit (Qiagen, Venlo, The Netherlands), according to the manufacturer's protocol. DNA from all probands underwent WES using a Twist Human Core Exome Kit and an Illumina NovaSeq 6000 sequencing system (150PE) (Berry Genomics Institute, Beijing, China). The mean depth and coverage of the target region were approximately 78.26× and 99.7%, respectively. Sequence reads were aligned to the reference human genome (UCSC hg19) using the Burrows-Wheeler aligner (BWA). The variants were called and annotated with Verita Trekker and Enliven software (Transcript ID, ENST00000332127.4, Berrry Genomics Institute), respectively.

Het-KO mice model construction, husbandry and ocular biometric measurements

The germline heterozygous *Zc3h11a* knockout (Het-KO) mice were generated by CRISPR/Cas9-mediated gene editing at the embryonic stage on a C57BL/6J background, provided by GemPharmatech Co., Ltd (Nanjing, China). Exon5-exon6 of the *Zc3h11a* transcript was recommended as the KO region; this region contains a 244bp coding sequence. Littermates of Het-KO and WT mice were used for all experiments. Phenotypic analyses were initiated when the mice reached four weeks of age. All animals were housed in the animal husbandry room of Wenzhou Medical University. Mice were housed in standard transparent mouse cages at 22±2°C with a 12-hour light/12-hour dark cycle (light from 8 am to 8 pm, brightness approximately 200-300 lux) and free access to food and water. To exclude potential confounding

361 effects of spontaneous ocular developmental abnormalities, a total of 7 mice (4 Het-KO
362 and 3 WT) with small eyes or ocular lesions were excluded from the observation cohort.
363 These anomalies were consistent with the baseline incidence of spontaneous
364 malformations observed in historical colony data of wild-type C57BL/6J mice
365 (approximately 11%), and were not attributed to the *Zc3h11a* heterozygous knockout.
366 Refractive measurements were performed by a researcher blinded to the genotypes.
367 Briefly, in a darkroom, mice were gently restrained by tail-holding on a platform facing
368 an eccentric infrared retinoscope (EIR) (Schaeffel et al., 2004; Zhou et al., 2008a). The
369 operator swiftly aligned the mouse position to obtain crisp Purkinje images centered on
370 the pupil using detection software (Schaeffel et al., 2004), enabling axial measurements
371 of refractive state and pupil size. Three repeated measurements per eye were averaged
372 for analysis. The anterior chamber (AC) depth, lens thickness, vitreous chamber
373 (VC)depth, and axial length (AL) of the eye were measured by real-time optical
374 coherence tomography (a custom built OCT) (Zhou et al., 2008b). In simple terms, after
375 anesthesia, each mouse was placed in a cylindrical holder on a positioning stage in front
376 of the optical scanning probe. A video monitoring system was used to observe the eyes
377 during the process. Additionally, by detecting the specular reflection on the corneal
378 apex and the posterior lens apex in the two dimensional OCT image, the optical axis of
379 the mouse eye was aligned with the axis of the probe. Eye dimensions were determined
380 by moving the focal plane with a stepper motor and recording the distance between the
381 interfaces of the eyes. Then, using the designed MATLAB software and appropriate
382 refractive indices, the recorded optical path length was converted into geometric path
383 length. Each eye was scanned three times, and the average value was taken. Body
384 weight, refraction and ocular biometrics of Het-KO (n=14) and WT (n=10) mice were
385 assessed at 4, 5, 6, 8 and 10 weeks of age.
386
387 **Electroretinography**
388 To evaluate the effect of *Zc3h11a* on the electrophysiological properties of various
389 neuronal populations in the retina, ERG was performed on the right eye of Het-KO and
390 WT littermates at seven weeks of age, at the same time of day (n=12). Both scotopic

and photopic ERG responses were evaluated. The mice were dark-adapted overnight, and all procedures were performed under dim red light (<1 lux). The animals were anaesthetized with intraperitoneal injection of pentobarbital sodium (40 mg/kg) and the pupils were dilated with 0.5% tropicamide. A heating table (37°C) was used to maintain body temperature. ERG was recorded using a Roland Electrophysiological System (RETI-Port21, Roland Consult, Germany) with ring-shaped corneal electrodes. Scotopic ERG responses were measured under the following parameters: 2.02 log cd·s/m² (dark 0.01): Extremely low light intensity, assessing rod cell function. 0.48 log cd·s/m² (dark 3.0): Moderate light intensity, evaluating the rod-bipolar cell pathway. 0.98 log cd·s/m² (dark 10.0): Higher light intensity, examining bipolar cell responses under strong stimulation. For photopic ERG responses, after 10 minutes of light adaptation at 25 cd·s/m², recordings were performed at 0.48 log cd·s/m² (light 3.0). Measured parameters included: a-wave amplitude (reflecting photoreceptor function). b-wave amplitude (indicating bipolar cell activity). The responses of the Het-KO eyes (right) were compared with those of the WT eyes (right).

Immunofluorescence

Whole mouse eyes (10 weeks, littermates Het-KO and WT) were fixed with 4% para-formaldehyde (BL539A, Biosharp, China) for 1 h and 30% sucrose for dehydration overnight. Then, they were fabric-embedded in a frozen fabric matrix compound at -20°C. Prepared tissue blocks were segmented with a cryostat at a thickness of 12 microns and collected on clean adhesive slides. The slices containing the sections were air-dried at room temperature (RT) for 15 min. After washing 3× with 1× PBS for 5 min, 5% BSA (SW3015, Solarbio, China) and 0.03% triton-X100 (P0096, Beyotime, China) diluted with 1× PBS were added as permeable membrane-blocking buffers. The slides were incubated for 1 h at RT in a humid chamber. Then, they were incubated overnight at 4°C with the specific primary antibody Zc3h11a (1:50, 26081, Proteintech, USA). PKC α (1:200, ab32518, Abcam, UK), Opsin-1 (1:200, NB110-74730, Novus Biologicals, USA) and Rhodopsin (1:200, NBP2-25160, Novus Biologicals, USA) were added and the slices were incubated further at 4°C in a humid chamber overnight.

After washing 4× with 1× PBS for 6 min, goat anti-rabbit Alexa Fluor 488 (1:500, ab150077, Abcam, UK) was added and the slides were incubated for 90 min at RT. After washing, the slides were mounted with an antifade medium containing DAPI (P0131, Beyotime, China) to visualize the cell nucleus. Sections incubated with 5% BSA and without primary antibodies were used as negative controls. A fluorescence microscope (LSM 880, ZEISS, Germany) was used to examine the slides and capture images. The experiments were repeated in duplicate with three different samples. Fluorescence intensity statistics were analyzed using ZEISS ZEN 3.4 software.

Transmission electron microscopy

At 10 weeks of age, two mice of each genotype were euthanized, and their eyes were removed. The eyes were fixed in a solution containing 2.5% glutaraldehyde and 0.01 M phosphate buffer (PB) (pH 7.0-7.5) for 15 min while the optic cups were dissected. The optic cups were then fixed with 1% osmium acid at room temperature away from light for 2h, after which they were rinsed three times with 0.1 MPB for 15min each time. Tissues were sequentially dehydrated in 30%-50%-70%-80%-95%-100%-100% ethanol upstream for 20 min each time, and 100% acetone twice for 15 min each time. Finally, the tissues were embedded in epoxy resin (Polybed 812) mixed 1:1 with acetone. Ultrathin sections were prepared using diamond knives and an EM UC7 ultramicrotome (Leica, Germany), then the sections were stained with 2% aqueous dioxygen acetate and 1% phosphotungstic acid (pH 3.2). Finally, the structures were examined using a transmission electron microscope (HT7700, Hitachi, Tokyo, Japan).

Cell culture, plasmid construction and transfected

HEK293T cell line (from Chinese Academy of Sciences) was cultured in DMEM medium containing 10% high-quality 10% fetal bovine serum (FBS) and 1% penicillin streptomycin dual antibody. Using restriction endonucleases HindIII and EcoRI to cleave the target gene product (wild type, *ZC3H11A*^{V138I}, *ZC3H11A*^{G43E}, *ZC3H11A*^{P154L} and *ZC3H11A*^{S747T}) and vector pcDNA3.1 (+), and purify the fragments. Then, under the action of T4 DNA ligase, the target gene was ligated with the vector pcDNA3.1 (+), and the ligated product was transformed into competent bacterial cells. Sequencing was

451 used to identify and select the successfully constructed target gene expression plasmid
452 vector. Finally, a sufficient amount of vector plasmids were obtained through ultrapure
453 endotoxin extraction. Transfected with wild type, *ZC3H11A*^{V138I}, *ZC3H11A*^{G43E},
454 *ZC3H11A*^{P154L} and *ZC3H11A*^{S747T} overexpression plasmids using NDE3000 reagent
455 (Western, China).
456
457 **RNA sequencing analysis of molecular and pathway changes in the mouse retina**
458 Retinas were harvested from four-week-old mice for RNA sequencing. Specifically,
459 mice at four weeks of age were euthanized via CO_2 asphyxiation followed by cervical
460 dislocation. Eyes were immediately enucleated and dissected to isolate intact retinas.
461 Three retinas per group (*Zc3h11a* Het-KO and WT) were processed for transcriptomic
462 analysis by Biomarker Biotechnology Co. (Beijing, China). The RNA sequences were
463 mapped to the genome (GRCm38). WebGestalt (http://www.webgestalt.org/) was used
464 to generate GO terms and KEGG pathways.
465
466 **RNA extraction and qRT-PCR**
467 To determine the reliability of the transcriptome results, qPCR validation was
468 performed. Total RNA and nuclear RNA were extracted using Trizol reagent (RC112,
469 Vazyme, China) and Cytodynamic & Nuclear RNA Purification Kit (21000, Norgen
470 Biotek, Canada), respectively, and the purity was confirmed by the OD260/280 nm
471 absorption ratio (1.9-2.1) (Nanodrop 2000, Thermo Scientific, USA). Total RNA (2 μg)
472 was reverse transcribed to cDNA using a cDNA Synthesis Kit (R323, Vazyme, China).
473 qPCR was performed with a RT-PCR detection system (Applied Biosystems, California,
474 USA) using a SYBR Premix Ex Taq Kit (Q711, Vazyme, China), according to the
475 manufacturer's instructions. qRT-PCR was performed (ABI-Q6, California, USA) in a
476 20 μL reaction, under the following conditions: 95°C for 10 min, followed by 40 cycles
477 of amplification at 95°C for 10 s and 60°C for 60 s. Melting curve analysis was used to
478 determine specific amplification. All experiments were performed in triplicate. Relative
479 quantification was performed using the ΔΔCt method. The specific gene products were
480 amplified using the following primer pairs (Supplement Table 1).

481

482 **Western blot**

483 The mouse retina was separated immediately after enucleation of the eyeball and lysed
484 in RIPA (10 mM Tris-Cl, 100 mM NaCl, 1 mM EDTA, 1 mM NaF, 20 mM $Na_4P_2O_7$,
485 2 mM Na_3VO_4, 1% Triton X-100, 10% glycerol, 0.1% sodium dodecyl sulphate and
486 0.5% deoxycholate) lysis buffer containing protease and phosphatase inhibitors (P1045,
487 Beyotime, China). Equal amounts of protein (15 μg) were separated on 10% Tris-
488 glycine gel, transferred to PVDF (polyvinylidene fluoride) membranes, and blocked
489 with 5% skim milk. The primary antibodies used included ZC3H11A (ab99930, Abcam,
490 UK), AKT (#4691, Cell Signaling Technology, USA), p-AKT (#4060, Cell Signaling
491 Technology, USA), IκBα (ab32518, Abcam, UK), NF-κB (ab32536, Abcam, UK),
492 TGF-β1 (21898, Proteintech, USA), PKCα (ab32518, Abcam, UK) and MMP-2
493 (ab92536, Abcam, UK) diluted to 1:1000 in TBST-5% milk. Then, the membranes were
494 incubated with goat anti-rabbit IgG conjugated with HRP (1:2000 in TBST-5% milk)
495 (SA00001-2, Proteintech, USA) for 90 min at room temperature and developed using
496 western blotting reagents (BL523B, Bioshark, China). GAPDH (AF2823, Byotime,
497 China) was used as the internal control.

498

499 **Software and statistical analysis**

500 All experiments were repeated at least once, and sample sizes and reported results
501 reflect the cumulative data for all trials of each experiment. Each result is expressed as
502 the mean ± standard deviation (SD). Pearson's test was used to assess the normality of
503 the data. The normally distributed data were subjected to parametric analyses. Unpaired
504 Student's t-tests were used for parametric analyses between two groups. Data that were
505 not normally distributed or had a sample size that was too small, were subjected to
506 nonparametric analyses. Nonparametric tests between two groups were performed
507 using the Wilcoxon signed-rank test for matched pairs, the Mann-Whitney U-test or the
508 Kruskal-Wallis test for multiple comparisons (GraphPad Prism 9, La Jolla, CA). A
509 difference was considered statistically significant when the p-value was less than 0.05
510 and highly significant if it was less than 0.01 or less than 0.001.

Acknowledgements

The authors wish to thank all of the members of our lab. Additionally, we thank myopia and big data research group at Eye Hospital of Wenzhou Medical University for their technical assistance.

Additional information

Funding

This work was supported by the National Natural Science Foundation of China (82101176), the Natural Science Foundation of Zhejiang Province (LTGD23H120002), the Health Technology Plan Project in Zhejiang Province (2023KY151) and the Science and Technology Project of Wenzhou (Y20220774)

Author Contributions

Conceptualisation, Xinting Liu, Jia Qu and Fan Lu; methodology, Chong Chen, Qian Liu and Cheng Tang; data analysis, Chong Chen, Qian Liu, Cheng Tang and Yu Rong; investigation and cohort construction, Xinting Liu, Jia Qu, Fan Lu, Dandan Li and Xinyi Zhao; writing original draft preparation, Chong Chen, Qian Liu and Xinting Liu; writing-review and editing, Xinting Liu, Jia Qu and Fan Lu; funding acquisition, Xinting Liu, Jia Qu and Fan Lu. All authors have read and agreed to the published version of the manuscript.

Ethics approval

The study was approved by the Institutional Review Board of Eye Hospital, Wenzhou Medical University, Zhejiang, China (REC reference 2021-015-K-12-01). Informed consent was obtained from each subject. The study was approved by the Animal Care and Ethics Committee at Wenzhou Medical University (Wenzhou, China).

Data availability

All data generated or analysed during this study are included in the manuscript and supporting files.

References

Alzahrani, A.S., 2019. PI3K/Akt/mTOR inhibitors in cancer: At the bench and bedside. Semin Cancer Biol 59, 125-132.

Baird, P.N., Saw, S.M., Lanca, C., Guggenheim, J.A., Smith Iii, E.L., Zhou, X., Matsui, K.O., Wu, P.C., Sankaridurg, P., Chia, A., Rosman, M., Lamoureux, E.L., Man, R., He, M., 2020. Myopia. Nat Rev Dis Primers 6, 99.

Baron, V., Adamson, E.D., Calogero, A., Ragona, G., Mercola, D., 2006. The transcription factor Egr1 is a direct regulator of multiple tumor suppressors including TGFbeta1, PTEN, p53, and fibronectin. Cancer Gene Ther 13, 115-124.

Cai, X.-B., Zheng, Y.-H., Chen, D.-F., Zhou, F.-Y., Xia, L.-Q., Wen, X.-R., Yuan, Y.-M., Han, F., Piao, S.-Y., Zhuang, W., Lu, F., Qu, J., Yu, A.Y., Jin, Z.-B., 2019. Expanding the Phenotypic and Genotypic Landscape of Nonsyndromic High Myopia: A Cross-Sectional Study in 731 Chinese Patients. Invest Ophthalmol Vis Sci 60, 4052-4062.

Chen, B.-Y., Wang, C.-Y., Chen, W.-Y., Ma, J.-X., 2013. Altered TGF-β2 and bFGF expression in scleral desmocytes from an experimentally-induced myopia guinea pig model. Graefes Arch Clin Exp Ophthalmol 251, 1133-1144.

Chen, C.-S., Hsu, Y.-A., Lin, C.-H., Wang, Y.-C., Lin, E.-S., Chang, C.-Y., Chen, J.J.-Y., Wu, M.-Y., Lin, H.-J., Wan, L., 2022. Fallopia Japonica and Prunella vulgaris inhibit myopia progression by suppressing AKT and NFκB mediated inflammatory reactions. BMC Complement Med Ther 22, 271.

Darweesh, M., Younis, S., Hajikhezri, Z., Ali, A., Jin, C., Punga, T., Gupta, S., Essand, M., Andersson, L., Akusjärvi, G., 2022. ZC3H11A loss of function enhances NF-κB signaling through defective IκBα protein expression. Frontiers in Immunology 13, 1002823.

Dyson, H.J., Komives, E.A., 2012. Role of disorder in IκB-NFκB interaction. IUBMB Life 64, 499-505.

Fan, Q., Barathi, V.A., Cheng, C.-Y., Zhou, X., Meguro, A., Nakata, I., Khor, C.-C., Goh, L.-K., Li, Y.-J., Lim, W.e., Ho, C.E.H., Hawthorne, F., Zheng, Y., Chua, D., Inoko, H., Yamashiro, K., Ohno-Matsui, K., Matsuo, K., Matsuda, F., Vithana, E., Seielstad, M., Mizuki, N., Beuerman, R.W., Tai, E.S., Yoshimura, N., Aung, T., Young, T.L., Wong, T.-Y., Teo, Y.-Y., Saw, S.-M., 2012. Genetic variants on chromosome 1q41 influence ocular axial length and high myopia. PLoS Genet 8, e1002753.

Flitcroft, D.I., He, M., Jonas, J.B., Jong, M., Naidoo, K., Ohno-Matsui, K., Rahi, J., Resnikoff, S., Vitale, S., Yannuzzi, L., 2019. IMI - Defining and Classifying Myopia: A Proposed Set of Standards for Clinical and Epidemiologic Studies. Invest Ophthalmol Vis Sci 60, M20-M30.

Haarman, A.E.G., Thiadens, A.A.H.J., van Tienhoven, M., Loudon, S.E., de Klein, J.E.M.M.A., Brosens, E., Polling, J.R., van der Schoot, V., Bouman, A., Kievit, A.J.A., Hoefsloot, L.H., Klaver, C.C.W., Verhoeven, V.J.M., 2022. Whole exome sequencing of known eye genes reveals genetic causes for high myopia. Hum Mol Genet 31, 3290-3298.

Harper, A.R., Summers, J.A., 2015. The dynamic sclera: extracellular matrix remodeling in normal ocular growth and myopia development. Exp Eye Res 133, 100-111.

Hayden, M.S., Ghosh, S., 2011. NF-κB in immunobiology. Cell Res 21, 223-244.

Holden, B.A., Fricke, T.R., Wilson, D.A., Jong, M., Naidoo, K.S., Sankaridurg, P., Wong, T.Y.,

Naduvilath, T.J., Resnikoff, S., 2016. Global Prevalence of Myopia and High Myopia and Temporal Trends from 2000 through 2050. Ophthalmology 123, 1036-1042.

Ikeda, S.-I., Kurihara, T., Jiang, X., Miwa, Y., Lee, D., Serizawa, N., Jeong, H., Mori, K., Katada, Y., Kunimi, H., Ozawa, N., Shoda, C., Ibuki, M., Negishi, K., Torii, H., Tsubota, K., 2022. Scleral PERK and ATF6 as targets of myopic axial elongation of mouse eyes. Nat Commun 13, 5859.

Jimi, E., Fei, H., Nakatomi, C., 2019. NF-κB Signaling Regulates Physiological and Pathological Chondrogenesis. Int J Mol Sci 20.

Koga, M., Mizuno, Y., Watanabe, I., Kawakami, H., Goto, T., 2014. Role of VPAC2 receptor in monocrotaline-induced pulmonary hypertension in rats. J Appl Physiol (1985) 117, 383-391.

Krizaj, D., Copenhagen, D.R., 2002. Calcium regulation in photoreceptors. Frontiers in bioscience: a journal and virtual library 7, d2023.

Libermann, T.A., Baltimore, D., 1990. Activation of interleukin-6 gene expression through the NF-kappa B transcription factor. Mol Cell Biol 10, 2327-2334.

Lin, H.-J., Wei, C.-C., Chang, C.-Y., Chen, T.-H., Hsu, Y.-A., Hsieh, Y.-C., Chen, H.-J., Wan, L., 2016. Role of chronic inflammation in myopia progression: clinical evidence and experimental validation. EBioMedicine 10, 269-281.

Liu, S., Chen, T., Chen, B., Liu, Y., Lu, X., Li, J., 2022. Lrpap1 deficiency leads to myopia through TGF-β-induced apoptosis in zebrafish. Cell Commun Signal 20, 162.

Manavalan, B., Basith, S., Choi, Y.-M., Lee, G., Choi, S., 2010. Structure-function relationship of cytoplasmic and nuclear IκB proteins: an in silico analysis. PLoS One 5, e15782.

Morgan, M.J., Liu, Z.-g., 2011. Crosstalk of reactive oxygen species and NF-κB signaling. Cell Res 21, 103-115.

Qi, J., Pan, W., Peng, T., Zeng, L., Li, X., Chen, Z., Yang, Z., Xu, H., 2022. Higher Circulating Levels of Neutrophils and Basophils Are Linked to Myopic Retinopathy. Int J Mol Sci 24.

Saw, S.-M., Gazzard, G., Shih-Yen, E.C., Chua, W.-H., 2005. Myopia and associated pathological complications. Ophthalmic Physiol Opt 25, 381-391.

Schaeffel, F., Burkhardt, E., Howland, H.C., Williams, R.W., 2004. Measurement of refractive state and deprivation myopia in two strains of mice. Optometry and Vision Science 81, 99-110.

Schippert, R., Burkhardt, E., Feldkaemper, M., Schaeffel, F., 2007. Relative axial myopia in Egr-1 (ZENK) knockout mice. Invest Ophthalmol Vis Sci 48, 11-17.

Shi, Y., Li, Y., Zhang, D., Zhang, H., Li, Y., Lu, F., Liu, X., He, F., Gong, B., Cai, L., Li, R., Liao, S., Ma, S., Lin, H., Cheng, J., Zheng, H., Shan, Y., Chen, B., Hu, J., Jin, X., Zhao, P., Chen, Y., Zhang, Y., Lin, Y., Li, X., Fan, Y., Yang, H., Wang, J., Yang, Z., 2011. Exome sequencing identifies ZNF644 mutations in high myopia. PLoS Genet 7, e1002084.

Szczerkowska, K.I., Petrezselyova, S., Lindovsky, J., Palkova, M., Dvorak, J., Makovicky, P., Fang, M., Jiang, C., Chen, L., Shi, M., Liu, X., Zhang, J., Kubik-Zahorodna, A., Schuster, B., Beck, I.M., Novosadova, V., Prochazka, J., Sedlacek, R., 2019. Myopia disease mouse models: a missense point mutation (S673G) and a protein-truncating mutation of the Zfp644 mimic human disease phenotype. Cell Biosci 9, 21.

Tang, S.M., Li, F.F., Lu, S.Y., Kam, K.W., Tam, P.O.S., Tham, C.C., Pang, C.P., Yam, J.C.S., Chen, L.J., 2020. Association of the ZC3H11B, ZFHX1B and SNTB1 genes with myopia of different severities. Br J Ophthalmol 104, 1472-1476.

Tedja, M.S., Haarman, A.E.G., Meester-Smoor, M.A., Kaprio, J., Mackey, D.A., Guggenheim, J.A., Hammond, C.J., Verhoeven, V.J.M., Klaver, C.C.W., 2019. IMI - Myopia Genetics Report. Invest

Ophthalmol Vis Sci 60.
Tian, Q., Tong, P., Chen, G., Deng, M., Cai, T.e., Tian, R., Zhang, Z., Xia, K., Hu, Z., 2023. GLRA2 gene mutations cause high myopia in humans and mice. J Med Genet 60, 193-203.
Tkatchenko, A.V., Walsh, P.A., Tkatchenko, T.V., Gustincich, S., Raviola, E., 2006. Form deprivation modulates retinal neurogenesis in primate experimental myopia. Proc Natl Acad Sci U S A 103, 4681-4686.
Tkatchenko, T.V., Tkatchenko, A.V., 2019. Pharmacogenomic Approach to Antimyopia Drug Development: Pathways Lead the Way. Trends Pharmacol Sci 40, 833-852.
Tkatchenko, T.V., Troilo, D., Benavente-Perez, A., Tkatchenko, A.V., 2018. Gene expression in response to optical defocus of opposite signs reveals bidirectional mechanism of visually guided eye growth. PLoS Biol 16, e2006021.
Torrealba, N., Vera, R., Fraile, B., Martínez-Onsurbe, P., Paniagua, R., Royuela, M., 2020. TGF-β/PI3K/AKT/mTOR/NF-kB pathway. Clinicopathological features in prostate cancer. Aging Male 23, 801-811.
Ugarte, M., Osborne, N.N., 2001. Zinc in the retina. Progress in neurobiology 64, 219-249.
Wallman, J., Winawer, J., 2004. Homeostasis of eye growth and the question of myopia. Neuron 43, 447-468.
Wang, G.-B., Zhang, Q.-J., Xiao, X.-S., Li, J.-Z., Zhang, F.-S., Li, S.-Q., Li, W., Li, T., Jia, X.-Y., Guo, L., Guo, X.-M., 2004. [Variations of the zinc finger protein 161 gene in Chinese with or without high myopia]. Yi Chuan 26, 155-159.
Wu, K.-I.S., Schmid-Schönbein, G.W., 2011. Nuclear factor kappa B and matrix metalloproteinase induced receptor cleavage in the spontaneously hypertensive rat. Hypertension 57, 261-268.
Xiao, K., Chen, Z., He, S., Long, Q., Chen, Y., 2025. The role of NF-κB pathway and its regulation of inflammatory cytokines in scleral remodeling of form-deprivation mice model. Immunologic Research 73, 1-8.
Xiao, Q., Xiao, J., Liu, J., Liu, J., Shu, G., Yin, G., 2022. Metformin suppresses the growth of colorectal cancer by targeting INHBA to inhibit TGF-β/PI3K/AKT signaling transduction. Cell Death Dis 13, 202.
Yang, E., Yu, J., Liu, X., Chu, H., Li, L., 2023. Familial Whole Exome Sequencing Study of 30 Families With Early-Onset High Myopia. Invest Ophthalmol Vis Sci 64, 10.
Ye, M., Ma, Y., Qin, Y.-X., Cai, B., Ma, L.-M., Ma, Z., Liu, Y., Jin, Z.-B., Zhuang, W.-J., 2023. Mutational investigation of 17 causative genes in a cohort of 113 families with nonsyndromic early-onset high myopia in northwestern China. Mol Genet Genomics 298, 669-682.
Yoshida, M., Whitsett, J.A., 2006. Alveolar macrophages and emphysema in surfactant protein-D-deficient mice. Respirology 11 Suppl, S37-S40.
Younis, S., Jouneau, A., Larsson, M., Oudin, J.F., Adenot, P., Omar, J., Brochard, V., Andersson, L., 2023. Ablation of ZC3H11A causes early embryonic lethality and dysregulation of metabolic processes. Proc Natl Acad Sci U S A 120, e2216799120.
Younis, S., Kamel, W., Falkeborn, T., Wang, H., Yu, D., Daniels, R., Essand, M., Hinkula, J., Akusjärvi, G., Andersson, L., 2018. Multiple nuclear-replicating viruses require the stress-induced protein ZC3H11A for efficient growth. Proc Natl Acad Sci U S A 115, E3808-E3816.
Zhao, F., Zhou, Q., Reinach, P.S., Yang, J., Ma, L., Wang, X., Wen, Y., Srinivasalu, N., Qu, J., Zhou, X., 2018. Cause and Effect Relationship between Changes in Scleral Matrix Metallopeptidase-2 Expression and Myopia Development in Mice. Am J Pathol 188, 1754-1767.
Zhou, X., Shen, M., Xie, J., Wang, J., Jiang, L., Pan, M., Qu, J., Lu, F., 2008a. The development of the

refractive status and ocular growth in C57BL/6 mice. Investigative ophthalmology & visual science 49, 5208-5214.

Zhou, X., Xie, J., Shen, M., Wang, J., Jiang, L., Qu, J., Lu, F., 2008b. Biometric measurement of the mouse eye using optical coherence tomography with focal plane advancement. Vision research 48, 1137-1143.

686 **Table 1 The clinical features and mutations of affected patients**

Patient information			Refraction (D)		Axial length (mm)		Variation information			Prediction software and databases				
ID.	Sex	Age	OD	OS	OD	OS	Genotype	chromosomal positions	Existing_variation (rs numbers)	SIFT (score)	PolyPhen2 (score)	CADD (score)	gnomAD	Clinvar
1	M	18	-6.50	-5.125	25.68	25.34	c.412G>A:p.Val138Ile, Het	chr1:203798692-203798692	rs142418357	D (0.03)	PB (0.912)	24.3	7.95E-06	-
2	F	15	-4.25	-6.125	24.61	25.11	c.128G>A:p.Gly43Glu, Het	chr1:203787771-203787771	-	D (0)	PS (0.906)	26	-	-
3	M	17	-8.00	-8.75	26.16	27.02	c.461C>T :p.Pro154Leu, Het	chr1:203798741-203798741	-	D (0)	PS (0.628)	29.3	-	-
4	F	15	-6.25	-3.70	25.53	24.86	c.2239T>A:p.Ser747Thr, Het	chr1:203821333-203821333	-	T (0.1)	PS (0.838)	22.7	-	-

687 M, male; F, female; Het, heterozygote; OD, ocular dexter; OS, oculus sinister; D, deleterious, T, tolerated; PB, probably_damaging; PS, possibly_damaging; gnomAD,
688 Genome Aggregation Database; AF, Allele Frequency; -, Not Applicable

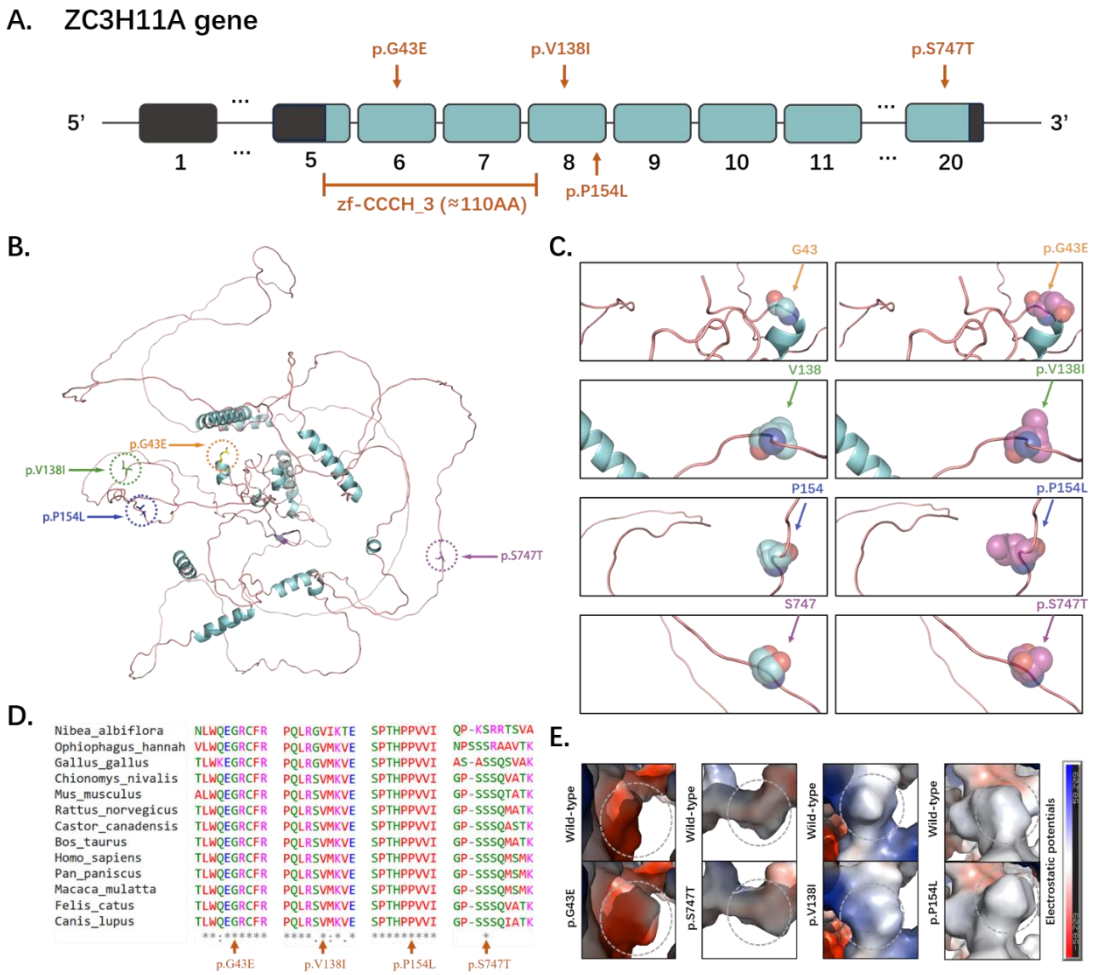

Figure 1. Structural and evolutionary analysis of *ZC3H11A* mutations in high myopia. (A) Enomic organization of *ZC3H11A*: Exon-intron structure (exons 1-20) with four identified missense mutations (orange arrows: c.128G>A/p.G43E, c.412G>A/p.V138I, c.461C>T/p.P154L, c.2239T>A/p.S747T). Domain architecture showing the zf-CCCH_3 zinc finger domain (exons 5-8) harboring three mutations (G43E, V138I, P154L). (B) Full-length ZC3H11A structural model: Predicted tertiary structure (PyMOL v2.5) with mutation sites highlighted: G43E (exon 6, orange), V138I/P154L (exon 8, green and blue), S747T (exon 20, purple). (C) Mutation localization: Schematic mapping of mutations to exons: G43E (exon 6), V138I/P154L (exon 8), S747T (exon 20). Exon sizes scaled proportionally. (D) Cross-species conservation: Multiple sequence alignment of *ZC3H11A* orthologs showing absolute conservation of mutated residues. (E) DynaMut2-predicted conformational flexibility changes: These mutations can result in a higher degree of conformational flexibility at the corresponding sites, potentially destabilizing the structural domain.

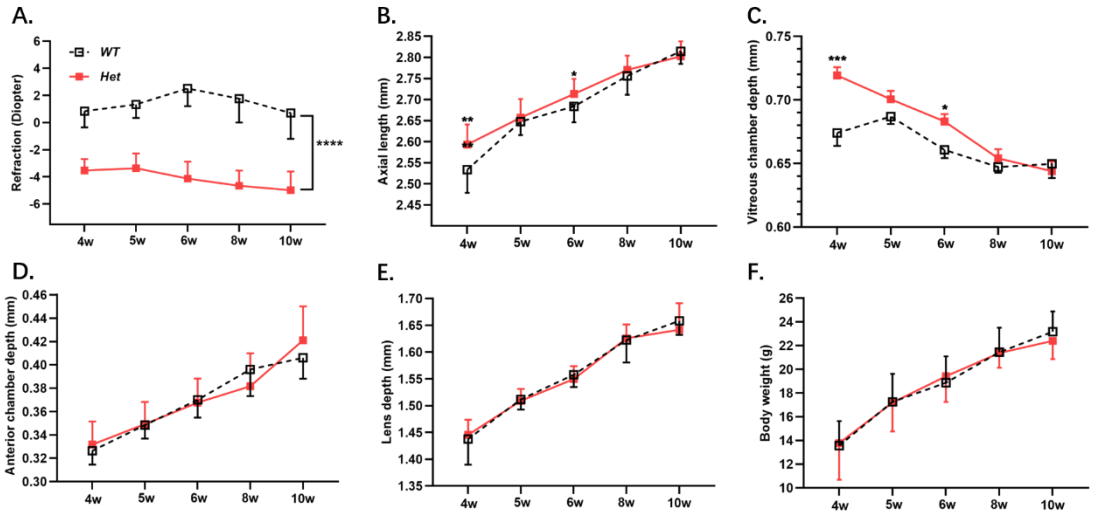

Figure 2. *Zc3h11a* Het-KO mice exhibit myopic shifts in refractive parameters. (A) Het-KO mice showed myopia in diopter. (B, C) Axial length and Vitreous chamber depth increased elongation in Het-KO mice at weeks 4 and 6. (D-F) No genotype-dependent differences in anterior chamber depth, lens thickness, or body weight. The effect of genotype on time-dependent refractive development was assessed through independent samples t-tests. P-values are indicated as follows: *P<0.05, **P<0.01, ***P<0.001 and ****<0.0001.

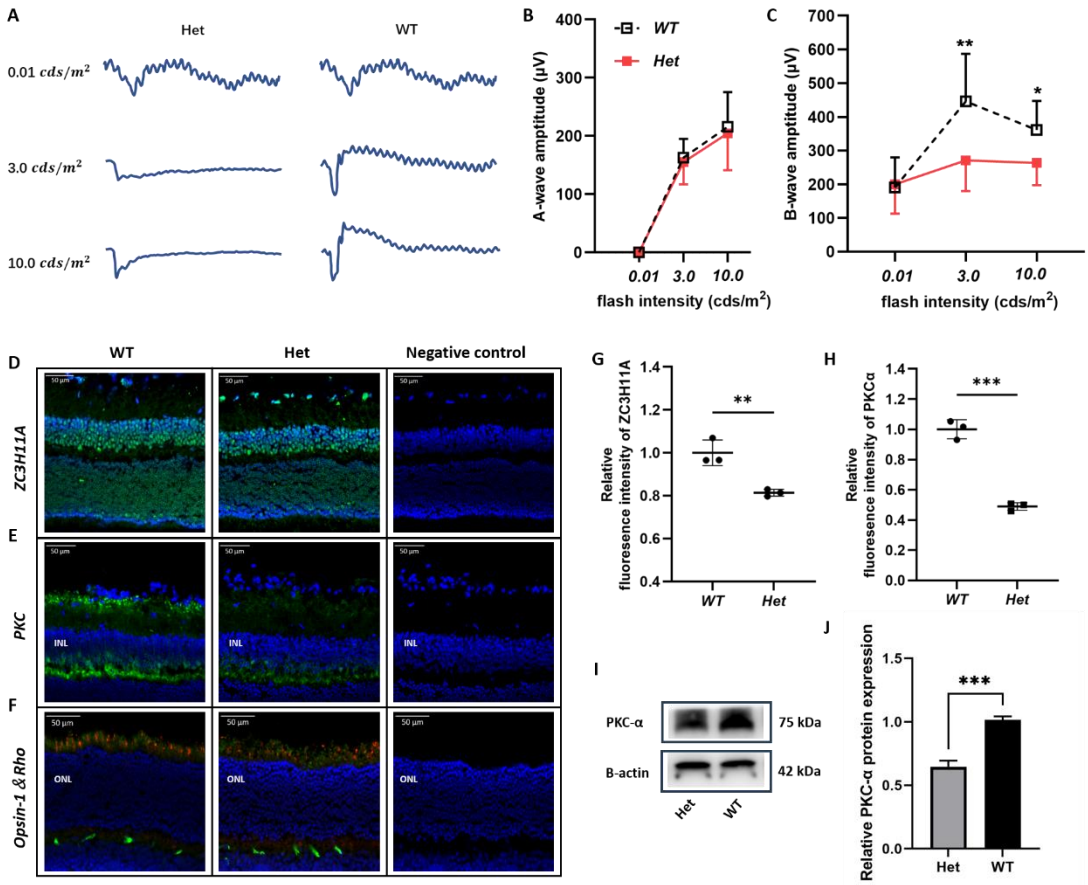

Figure 3. *Zc3h11a* Het-KO mice exhibited bipolar cell dysfunction, accompanied by reduced abundance of the key bipolar cell marker protein PKCα. (A) Representative scotopic ERG responses from Het-KO and WT eyes at dark 0.01(2.02 log cd·s/m²), dark 3.0 (0.48 log cd·s/m²and 10.0 (0.98 log cd·s/m²). (B, C) Quantification of a-wave (photoreceptor function) and b-wave (bipolar cell function) amplitudes. Het-KO mice (n=12) show significant b-wave reduction at dark 3.0 and dark 10.0 vs. WT (n=12). No a-wave differences observed (p>0.1). (D-F) Immunofluorescence-stained samples to detect Zc3h11a, PKCα (key bipolar cell marker protein), Opsin-1 (key cone photoreceptors marker protein) and Rhodopsin (key rod photoreceptors marker protein). (G, H) Zc3h11a and PKCα protein abundance reduced in the retina of Het-KO mice. (I) Western blot analysis showed that the PKCα protein content in the retina of Het-KO mice was decreased. (J) No differences in Opsin-1 or Rhodopsin protein abundance. Statistical significance was defined as *P < 0.05, **P<0.01 and ***P<0.001, as determined by independent samples t-tests.

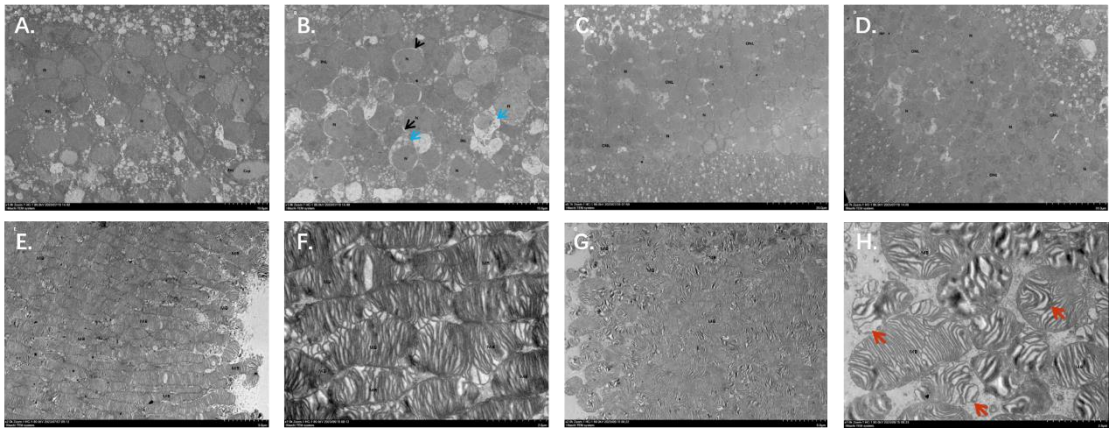

Figure 4. TEM showing the retinal abnormalities ultrastructure of *Zc3h11a* Het-KO mice. (A-B) Inner nuclear layer (INL). (A) WT mice, normal bipolar cell morphology; (B) *Zc3h11a* Het-KO pathological features include enlarged perinuclear gaps (black arrowheads), cytoplasmic edema (blue arrowheads), thinned/lightened cytoplasm in bipolar cells. (C-D) Outer nuclear layer (ONL). (C) WT mice and (D) *Zc3h11a* Het-KO mice Het-KO, no significant differences in photoreceptor nucleus morphology. (E-H) Photoreceptor membrane discs (MB). (E-F) WT mice, tightly stacked, uniformly arranged membrane discs. (G-H) *Zc3h11a* Het-KO structural disruptions include the outer layer falls off, the local distribution is sparse, and the arrangement is chaotic and loose (red arrow).

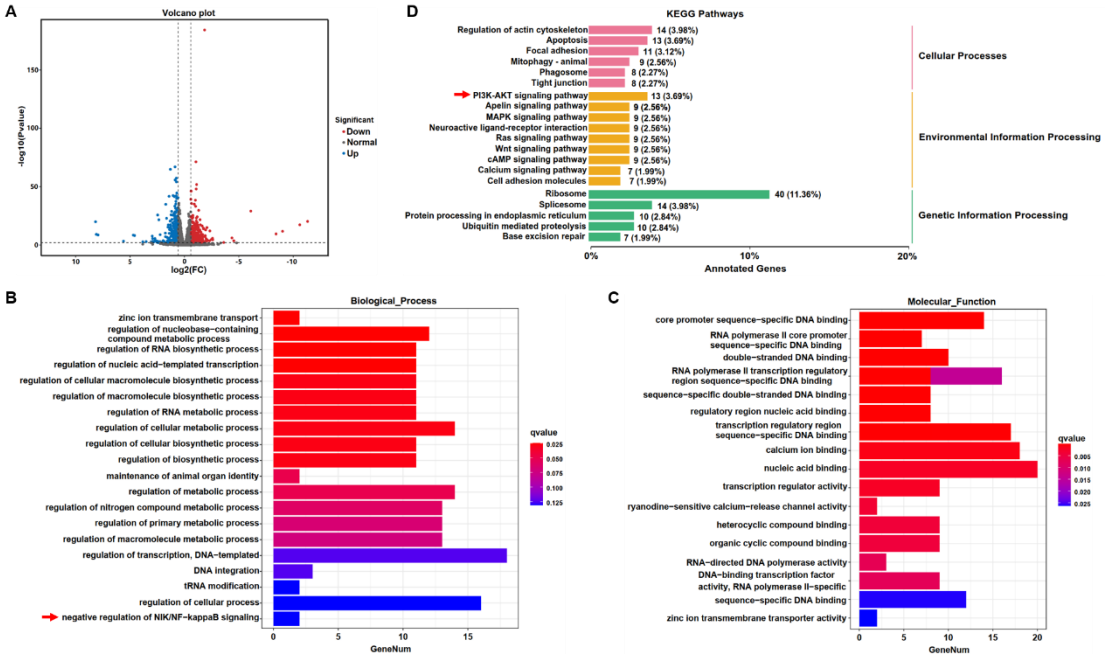

Figure 5. RNA-Seq reveals pathway dysregulation in the retina of *Zc3h11a* Het-KO mice. (A) Volcano plot of differentially expressed genes (DEGs): 769 total (303 upregulated, 466 downregulated in Het-KO vs. WT retinas. (B, C) Gene Ontology (GO)

enrichment analysis: Biological Process: Zinc ion transmembrane transport (GO: 0071577, photoreceptor maintenance), Negative regulation of NF-κB signaling (GO: 0043124, scleral remodeling). Molecular Function: Calcium ion binding (GO: 0005509, phototransduction), Zinc ion transmembrane transporter activity (GO: 0005385, retinal zinc homeostasis). (D) KEGG pathway enrichment analysis: Key pathways: PI3K-AKT signaling, MAPK signaling.

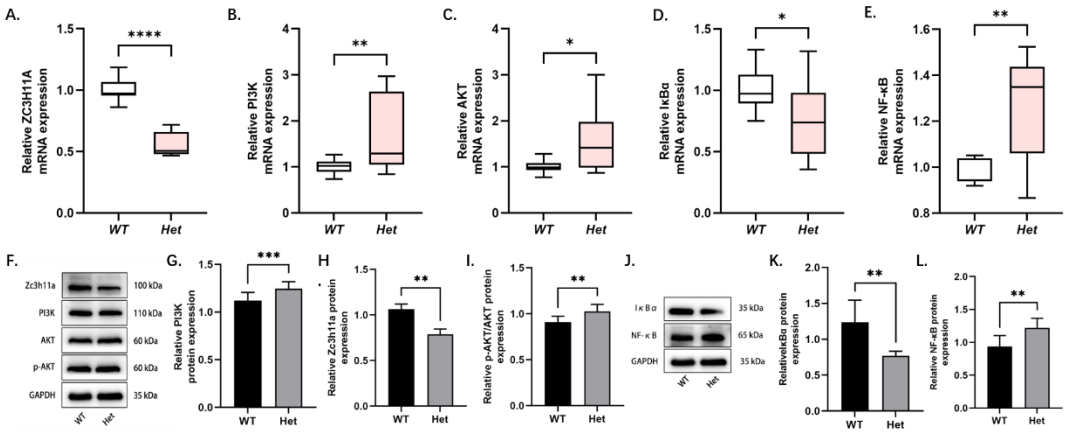

Figure 6. Dysregulation of PI3K-AKT and NF-κB signaling pathways in the retinas of *Zc3h11a* heterozygous knockout (Het-KO) mice. (A-E) qRT-PCR quantification of *ZC3H11A, PI3K, AKT, IκBα*, and *NF-κB* mRNA in the retina (n=3 mice/group): *Zc3h11a* expression was decreased in *Zc3h11a* Het-KO mouse retinas, while *PI3K* and *AKT* expression were increased; *IκBα* expression was decreased and *NF-κB* expression was increased. (F-L) Western blot analysis of Zc3h11a, PI3K, p-AKT/AKT, IκBα, and NF-κB protein levels in the retina (n=3 mice/group). (F-I) Quantitative analysis of ZC3H11A and PI3K levels normalized to GAPDH, while p-AKT levels were normalized to AKT: ZC3H11A expression was decreased in *Zc3h11a* Het-KO mouse retinas, while PI3K and p-AKT/AKT expression were increased. (J-L) Quantitative analyses of IκBα and NF-κB normalized to GAPDH: IκBα expression was decreased in *Zc3h11a* Het-KO mouse retinas.

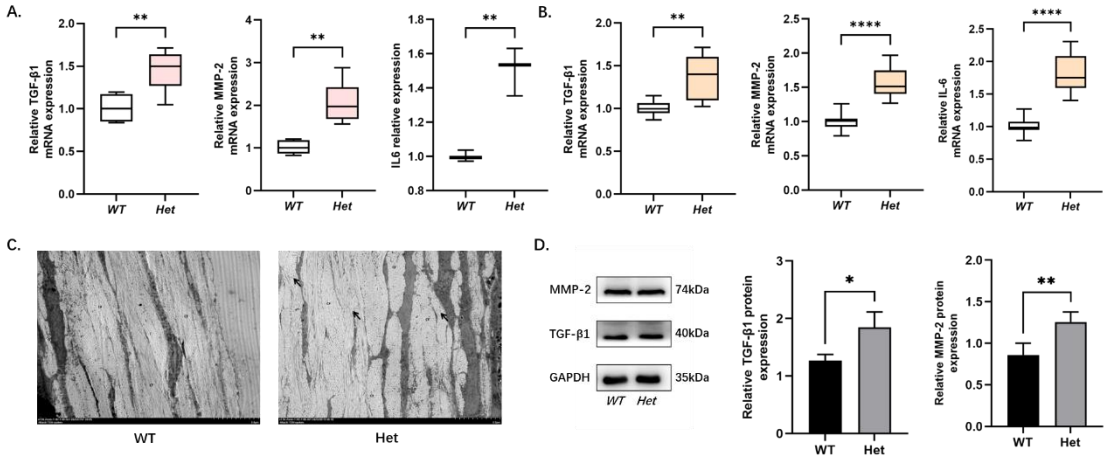

Figure 7. Elevated expression of TGF-β1, MMP-2, and IL-6 in retina and sclera of *Zc3h11a* Het-KO mice, with disrupted scleral ultrastructure. (A, B) qRT-PCR quantification of TGF-β1, MMP-2 and IL-6 mRNA in retina (A) and sclera (B) (n=3 mice/group): Expression of TGF-β1, MMP-2 and IL-6 was increased in both retina and sclera of Zc3h11a Het-KO mice. (C) TEM structure of sclera, WT mice, organized collagen fibers with regular transverse/longitudinal arrangement. *Zc3h11a* Het-KO mice, disorganized collagen fibers structure with irregular arrangement (black arrows). (D) Quantitative analyses of TGF-β1 and MMP-2 normalized to GAPDH (n=3 mice/group): Expression of TGF-β1 and MMP-2 was increased in retinas of Zc3h11a Het-KO mice.

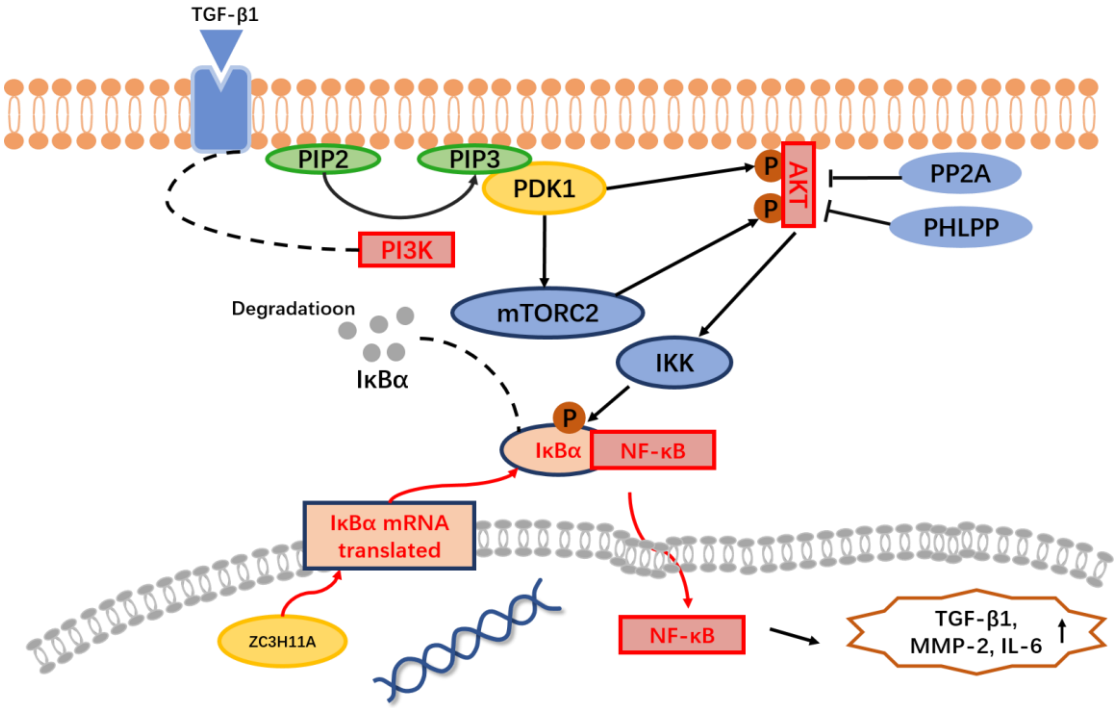

Figure 8. Mechanism of *Zc3h11a* haploinsufficiency-driven dysregulation of PI3K-AKT/NF-κB signaling in myopia pathogenesis. NF-κB activation, loss of *ZC3H11A* impairs nuclear export of IκBα mRNA, leading to reduced cytoplasmic IκBα protein levels and consequent hyperactivation of NF-κB. PI3K-AKT activation. *ZC3H11A* deficiency upregulates PI3K, enhancing the conversion of PIP2 to PIP3, which drives AKT phosphorylation (p-AKT). Activated p-AKT promotes IκBα degradation, further amplifying NF-κB nuclear translocation and transcriptional activity. Downstream effects, the combined hyperactivity of PI3K-AKT and NF-κB pathways elevates the expression of: TGF-β1 (extracellular matrix remodeling), MMP-2 (collagen degradation), IL-6 (pro-inflammatory signaling), collectively driving scleral thinning and inflammatory responses in myopia pathogenesis.

Supplementary files

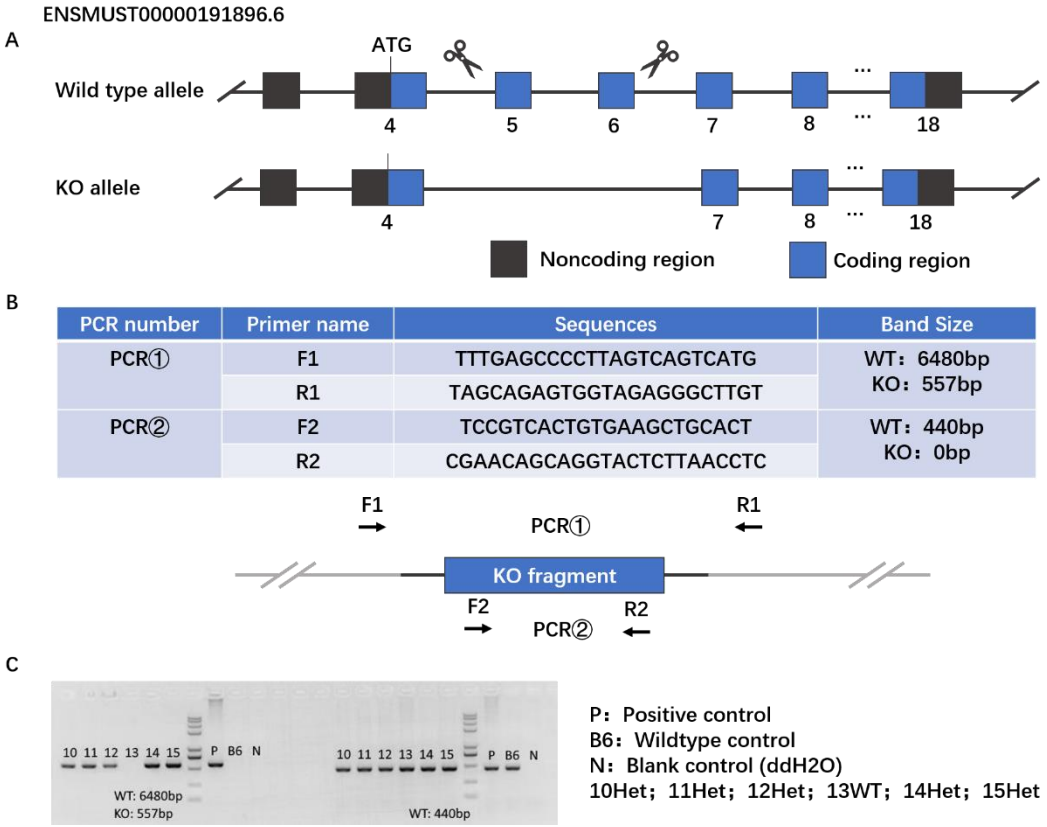

PCR number	Primer name	Sequences	Band Size
PCR①	F1	TTTGAGCCCCTTAGTCAGTCATG	WT：6480bp KO：557bp
	R1	TAGCAGAGTGGTAGAGGGCTTGT	
PCR②	F2	TCCGTCACTGTGAAGCTGCACT	WT：440bp KO：0bp
	R2	CGAACAGCAGGTACTCTTAACCTC	

Supplement Figure 1. Generation of *Zc3h11a* KO mice. (A) Generation of Zc3h11a KO mice in C57BL/6J background using CRISPR/Cas9 technology: Exon 5 to exon 6 of the *Zc3h11a* transcript was used as the KO region; this region contains a 244 bp coding sequence, and knocking out this region will result in loss of protein function (B-C) Primers for genotyping and examples of genotyping results of *Zc3h11a* Het-KO mice and wild-type mice.

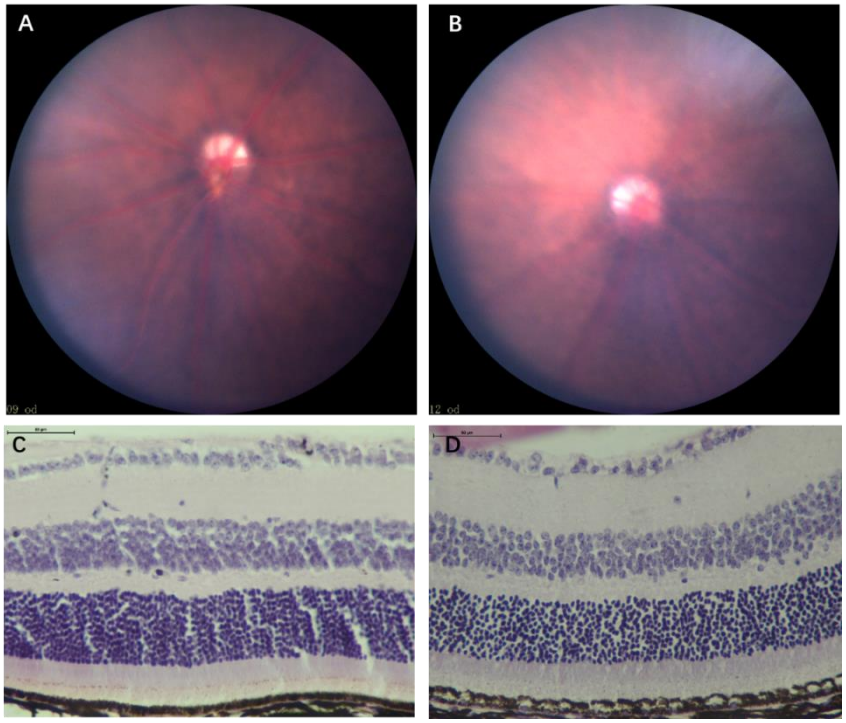

Supplement Figure 2. Fundus photographs and HE staining of Het and WT mice at 8th week. (A. B) There were no significant differences in fundus photographs between *Zc3h11a* Het-KO and WT mice, WT (A) and Het-KO mice (B) (n=3). (C. D) There were no significant differences in HE staining between *Zc3h11a* Het-KO and WT mice. WT (C) and Het-KO mice (D) (n=3).

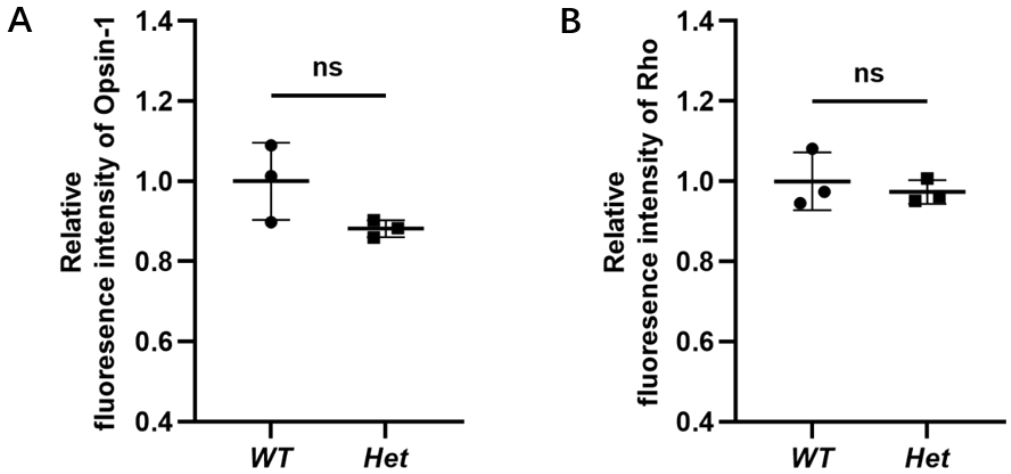

Supplement Figure 3. Quantitative analysis of cone cells and rod cells in Zc3h11a Het-KO. (A) No significance differences in Opsin-1 abundance. (B) No significance differences in Rhodopsin protein abundance.

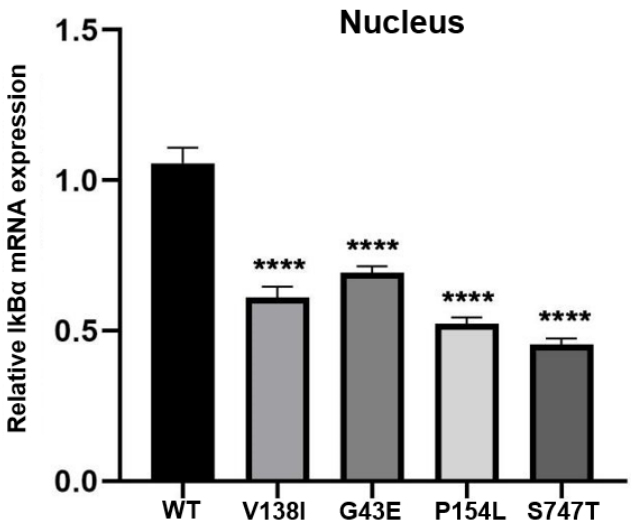

Supplement Figure 4. The relative mRNA expression levels of IκBα in the nucleus. Transfection of ZC3H11A overexpression mutant plasmid into cells resulted in a significant decrease in the mRNA expression levels of IκBα in four mutants ($ZC3H11A^{V138I}$, $ZC3H11A^{G43E}$, $ZC3H11A^{P154L}$ and $ZC3H11A^{S747T}$).

Supplement Table 1. Sequence of oligonucleotides

Gene	Sequence
ZC3H11A	Forward: CTAAACTGCGCTTTCCATCACA Reserve: CGTTGATTACAACAGGCGGAT
PI3K	Forward: TGGGACCTTTTTGGTACGAGA Reserve: AGCTAAAGACTCATTCCGGTAGT
AKT	Forward: CCTTTATTGGCTACAAGGAACGG Reserve: GAAGGTGCGCTCAATGACTG
IκBα	Forward: TGAAGGACGAGGAGTACGAGC Reserve: TGCAGGAACGAGTCTCCGT
NF-κB	Forward: GGGGCCTGCAAAGGTTATC Reserve: TGCTGTTACGGTGCATACCC
TGF-β1	Forward: GTAACGCCAGCCAGGAATTGTTGCTA Reserve: CTTCAATACGTCAGACATTCGGG
IL-6	Forward: CTGCAAGAGACTTCCATCCAG Reserve: AGTGGTATAGACAGGTCTGTTGG
MMP-2	Forward: CAAGTTCCCCGGCGATGTC Reserve: TTCTGGTCAAGGTCACCTGTC
GAPDH	Forward: AGGTCGGTGTGAACGGCTTTG Reserve: TGTAGACCATCTAGTTGAGGTCA

The mRNA expression levels were analysed by the comparative $2^{-\Delta\Delta}$ Ct method and normalised using GAPDH.